

Tracking an Aerodynamic Model in a Wind Tunnel with a Stereo High-speed Imaging System

Lichuan Gui, Nathan E Murray and John M Seiner

National Center for Physical Acoustics, University of Mississippi
Oxford, MS 38655, USA

Abstract— A method is presented to track the 3D motion of an aerodynamic model in wind tunnel tests with a stereo high-speed imaging system. The imaging system includes two high-speed cameras that work at 4,000 frames per second with a digital resolution of 1024×512 pixels. Stereo image recordings of tracking markers, which are precisely distributed on the model surface, are captured with a limited view angle difference between the two cameras. The stereo images are calibrated and 2D positions of tracking markers in the image frame are determined with a correlation-based algorithm. The camera positions and view angles are calibrated with a target shifting test. The determined 2D positions of both camera views in each stereo image recording are used to reconstruct instantaneous 3D coordinates of the tracking markers. A minimum quadratic difference approach is used to determine the center coordinates, roll angle, pitch angle and yaw angle of the aerodynamic model in the wind tunnel. Tests and simulations were conducted to verify the method.

Keywords- *Motion tracking, 3D imaging, stereo imaging, high-speed imaging, wind tunnel test, aerodynamic model*

I. INTRODUCTION

The stereo high-speed imaging technique is an ideal tool to investigate 3D motion of aerodynamic models in wind tunnel tests. The motion of an aerodynamic model are usually described with variables of model center coordinates (x_c, y_c, z_c) , roll angle ϕ , pitch angle θ , and yaw angle ψ . Surface markers are used to visualize the motion of the test model so that imaging techniques can be used to determine these variables for the motion of the model. A single high-speed camera with a stereo adaptor is a general configuration in most stereo high-speed imaging systems, e.g. [1] [2] [3] and [4]. However, two or more high-speed cameras are sometimes necessary to achieve a higher digital and temporal resolution, e.g. [5] and [6]. When using a two-camera stereo imaging system to investigate a marked model surface, image patterns of the surface markers are changed according to camera view angles and out-of-plane displacements. With known view angles, the image pattern difference between recordings of the two stereo cameras determines the out-of-plane displacement, so that 3D coordinates of the model surface markers can be obtained. A traditional way of processing a stereo image pair is to project the surface marker images of the two different camera views to a common measurement plane. When the 2D coordinates of a projected marker image are determined in the measurement plane for both camera views, the 3D coordinates

of the model surface marker can be reconstructed with the 2D data and the known view angles. A similar idea is used in a flow measurement technique, i.e. stereo particle image velocimetry (SPIV) [7], to determine 3D motion of tracer particles.

An aerodynamic model usually has a main axis, and a center that can be defined on the main axis, so that the marker positions on the model surface can be determined with a cylindrical coordinate system, i.e. axis coordinate L , radius R and angular position Φ . When the 3D coordinate data of the surface markers are obtained by evaluating the stereo image recordings, the model center coordinates, roll angle, pitch angle, and yaw angle can be determined with geometrical relations between the surface markers and the motion variables. Basically, three properly distributed surface markers are capable of determining the six motion variables, but more markers are required to achieve a high reliability and accuracy. When four or more surface markers are used for the motion tracking, a minimum quadratic difference approach can be used to solve the nonlinear equation system.

In this manuscript, the measurement system and details of the data reduction procedure are presented. A group of 120 stereo image recording pairs is synthetically generated and used to simulate the motion of the tested model, so that the accuracy of the stereo high-speed imaging tests can be estimated. More details will be presented in the conference.

II. MEASUREMENT SYSTEM AND DATA REDUCTION

A. Experimental Setup

A schematic illustration of a top view of the stereo high-speed imaging system is in Fig. 1. The system includes two Photron Ultima APX cameras that are capable of capturing stereo image pairs of the tested aerodynamic model in the wind tunnel with digital resolution of 1024×512 pixels at 4,000 frames per second through a glass window. A strobe light source is synchronized with the two cameras to provide sufficient illumination on the model surface. The test model has a length of 178 mm and a maximal diameter of 18 mm. According to previous 2D experiments, the motion of the test model can be investigated in a field of view of 305×152-mm². Two 60-mm Nikon Micro Nikkor lenses are selected for the cameras to achieve a deep focus region at a low image distortion. The measurement volume is determined with overlapping focus regions of the two cameras.

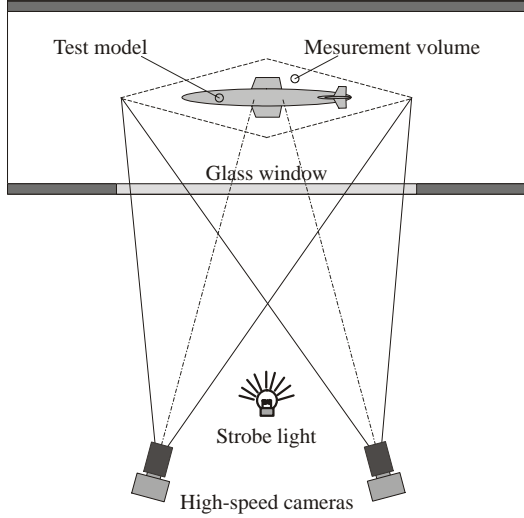


Figure 1. Schematic illustration of the top view of the stereo high-speed imaging system in a wind tunnel test

B. 3D Coordinate Reconstruction

The first step in processing the stereo image recordings is to transfer the distorted image to the undistorted target plane, which is centered in the measurement volume, with an image calibration algorithm. The available image calibration algorithms are described and discussed in a review paper for the stereo particle image velocimetry (SPIV) [7].

The markers on the test model surface are either spherical dots or intersections of grid lines whose positions can be tracked from frame to frame with an image pattern identification technique or a correlation-based image pattern tracking algorithm as described in [8] and [9].

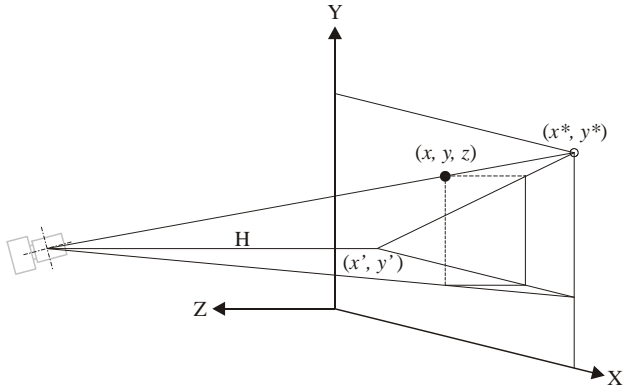


Figure 2. Physical and image coordinates

Fig. 2 shows the geometrical relations between physical coordinates (x, y, z) and image coordinates (x^*, y^*) for a camera whose position is determined by a target shifting test as (x', y', H) . When the 2D positions of a surface marker are determined in the target plane as (x_a, y_a) and (x_b, y_b) for the left (A) and right (B) camera, respectively, and the camera

positions are determined as (x'_a, y'_a, H_a) and (x'_b, y'_b, H_b) , the 3D coordinates (x, y, z) can be reconstructed as

$$\begin{cases} x = \frac{\frac{x_a - x'_a}{H_a} x_b - \frac{x_b - x'_b}{H_b} x_a}{\frac{x_a - x'_a}{H_a} - \frac{x_b - x'_b}{H_b}} \\ y = \frac{\frac{y_a - y'_a}{H_a} y_b - \frac{y_b - y'_b}{H_b} y_a}{\frac{y_a - y'_a}{H_a} - \frac{y_b - y'_b}{H_b}} \\ z = \frac{x_a - x_b}{\frac{x_a - x'_a}{H_a} - \frac{x_b - x'_b}{H_b}} \end{cases} \quad (1)$$

Note that coordinate z is determined only with data of x -coordinate because the main view angle difference between the stereo cameras is in xz -plane. When the center of the field of view is at (x_0, y_0, z_0) , the view angles of the camera are determined as

$$\begin{cases} \alpha = \tan^{-1}\left(\frac{x_0 - x'}{H}\right) \\ \beta = \tan^{-1}\left(\frac{y_0 - y'}{H}\right) \end{cases} \quad (2)$$

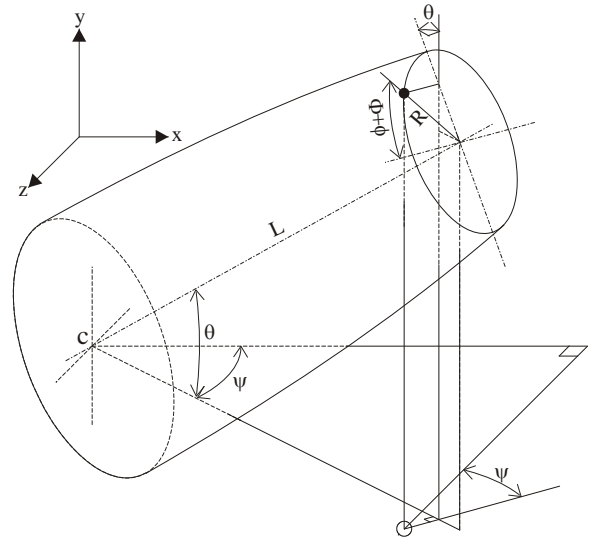


Figure 3. Local model coordinates and tracking variables

C. Tracking Variables

As shown in Fig. 3, a cylindrical coordinate system is used to determine the position of a surface marker on the tested model surface. With origin set at the model center on the main axis, the cylindrical coordinate system includes axis coordinate L , radius R and angular position Φ . A Cartesian coordinate system is used to determine model center position (x_c, y_c, z_c) ,

roll angle ϕ , pitch angle θ , and yaw angle ψ . The relation between the local model coordinates (L, R, Φ) and the global measurement coordinates (x, y, z) are represented as

$$\begin{cases} x = [L \cos \theta - R \sin(\phi + \Phi) \sin \theta] \cos \psi \\ \quad - R \cos(\phi + \Phi) \sin \psi + x_c \\ y = L \sin \theta + R \sin(\phi + \Phi) \cos \theta + y_c \\ z = [L \cos \theta - R \sin(\phi + \Phi) \sin \theta] \sin \psi \\ \quad + R \cos(\phi + \Phi) \cos \psi + z_c \end{cases} \quad (3)$$

When a group of surface markers of known local coordinates, i.e. (L_n, R_n, Φ_n) for $n=1,2,3,\dots,M$, are tracked in the measurement volume and the 3D coordinates of the surface markers are determined for certain stereo image recording as (x_n, y_n, z_n), the model center position (x_c, y_c, z_c) and angles ϕ, θ , and ψ can be determined with a two-step minimum quadratic difference approach.

D. Minimum Quadratic Difference Approach

According to the second equation in (3), the first-step quadratic difference function can be defined as

$$D_1(\theta, \phi) = \sum_{n=1}^M [y_c - y_n + L_n \sin \theta + R_n \sin(\phi + \Phi_n) \cos \theta]^2 \quad (4)$$

Wherein variable y_c is dependent on θ and ϕ , and it can be determined as

$$y_c = \frac{1}{M} \sum_{n=1}^M [y_n - L_n \sin \theta - R_n \sin(\phi + \Phi_n) \cos \theta] \quad (5)$$

Variable θ, ϕ and y_c can be determined by solving (4) and (5) at the minimum of function $D_1(\theta, \phi)$.

The second-step quadratic difference function can be defined with known value of θ and ϕ according to the first equation in (3) as

$$D_2(\psi) = \sum_{n=1}^M \{x_c - x_n - R_n \cos(\phi + \Phi_n) \sin \psi + [L_n \cos \theta - R_n \sin(\phi + \Phi_n) \sin \theta] \cos \psi\}^2 \quad (6)$$

Wherein variable x_c is dependent on ψ , and it can be determined as

$$x_c = \frac{1}{M} \sum_{n=1}^M \{x_n + R_n \cos(\phi + \Phi_n) \sin \psi - [L_n \cos \theta - R_n \sin(\phi + \Phi_n) \sin \theta] \cos \psi\} \quad (7)$$

Variable ψ and x_c can be determined by solving (6) and (7) at the minimum of function $D_2(\psi)$.

Finally, variable z_c can be determined with known values of ϕ, θ , and ψ as

$$z_c = \frac{1}{M} \sum_{n=1}^M \{z_n - R_n \cos(\phi + \Phi_n) \cos \psi - [L_n \cos \theta - R_n \sin(\phi + \Phi_n) \sin \theta] \sin \psi\} \quad (8)$$

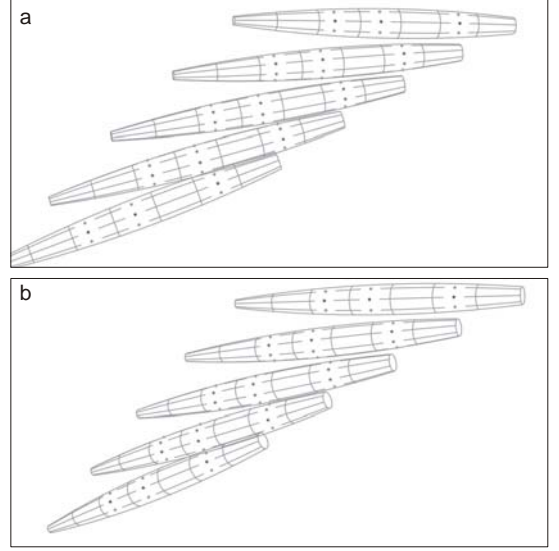


Figure 4. Synthetic stereo images overlapped every 30 frames: (a) from left camera, (b) from right camera.

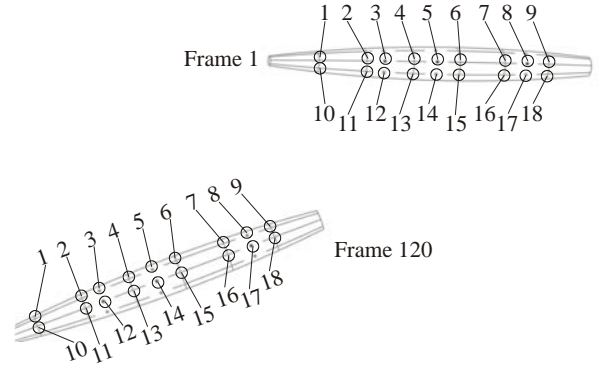


Figure 5. Available tracking marker images in the first frame (Frame 1) and the last frame (Frame 120)

III. SYNTHETIC IMAGE AND SIMULATED MOTION

In order to test the method and algorithms, a group of synthetic stereo image recording pairs are used to simulate a given motion of a revolving surface model. The model has a length of 177.8 mm (7 inches) and maximal diameter of 17.8 mm (0.7 inches) in the middle. The diameters at the two ends of the model are 7.62 mm (0.3 inches) and 10.16 mm (0.4

inches), respectively. The model moves in the x-direction at a constant speed of 5 m/s from the right to the left. In the y-direction the model has an initial speed of -3.33 m/s and an acceleration of -16.27 m/s^2 . The angular speed of roll, pitch, and yaw are 26.4, 11.7 and 5.9 radian/second. 120 stereo image recording pairs are generated with frame size of 1024×512 pixels for a field of view of $304.8 \times 152.4 \text{ mm}^2$ at a frame rate of 4000 fps. Grid lines of 0.25-mm thick are distributed on the simulated model with distance of 1 inch (25.4 mm) in the axis direction and with angular difference of 45° . Spherical dots of 1-mm diameter are put at the central cross-section replacing grid line intersections. Another two group of spherical dots are set at the revolving surface with the same radius of $R=7.96 \text{ mm}$ at $L=-28.58 \text{ mm}$ and $L=50.8 \text{ mm}$, respectively. The contrast of the spherical dots is the highest at $\phi+\Phi=0^\circ$, and it reduces linearly with increasing angular magnitude down to 50% at $\phi+\Phi=\pm 90^\circ$. The view angles of the left camera are set as $\alpha_a=15^\circ$ and $\beta_a=3^\circ$, whereas the right camera view angles are $\alpha_b=-22.5^\circ$ and $\beta_b=-2^\circ$. The stereo images are overlapped every 30 frames and shown in Fig. 4a and 4b for the left and right camera view, respectively.

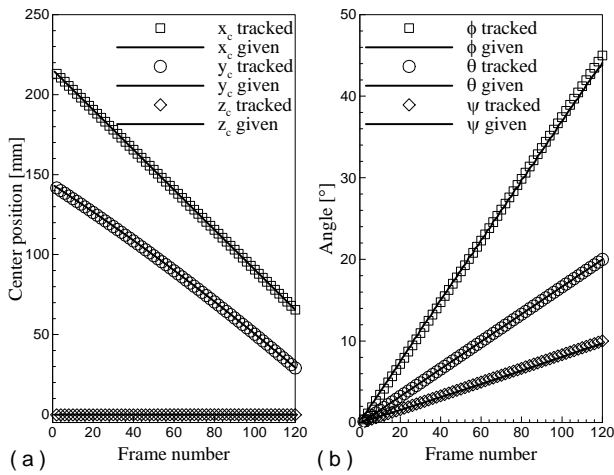


Figure 6. Tracking variables obtained from the 4-point motion tracking: (a) model center coordinates, (b) angles of the tested model

Because of the roll motion of the aerodynamic model, some surface marker images cannot be completely tracked from beginning to the end. The marker image contrast and the distance between neighbored marker images have significant influence on the tracking as well. The markers on the simulated model surface that can be identified not only in the first frame, but also in the last frame of the 120 synthetic stereo recordings are numbered and shown in Fig. 5 for the left camera view. As shown in Fig. 5, in the first frame, surface markers #1~#9 are close to the center line of the model image so that they can easy be tracked because of their high contrast and long distance to the neighbored marker images; whereas markers #10~#18 are near to the lower edge of the model image with lower contrast and shorter distance to the neighbors, so that the tracking uncertainty may increase at some of the tracked markers, e.g. #10, #11 and #18. When the model rolls by 45° in the last frame (Frame 120), surface markers #1~#9 turn to the side with reduced contrast and short distance to the neighbored marker

images, so that tracking uncertainty may increase, especially at #1, #2 and #9.

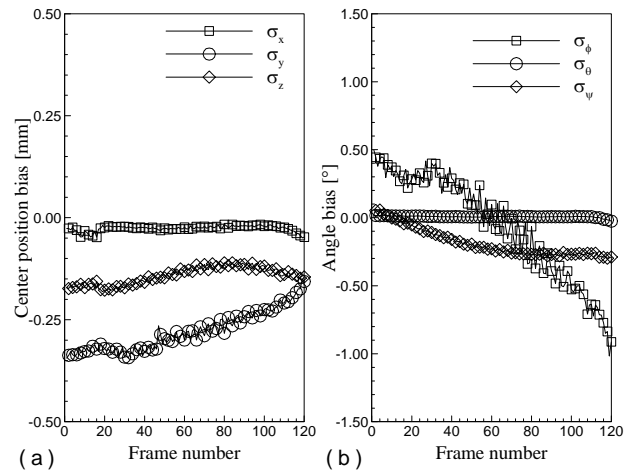


Figure 7. Tracking biases determined for the 4-point motion tracking: (a) model center coordinates, (b) angles of the tested model

TABLE I. TRACKING WITH DIFFERENT MARKERS

Group	Number	Marker numbers as shown in Fig. 5
1	3	3,8,14
2	4	3,5,8,14
3	6	3,5,8,12,14,17
4	8	3,5,6,8,12,14,15,17
5	10	3,4,5,6,8,12,13,14,15,17
6	12	3,4,5,6,7,8,12,13,14,15,16,17
7	14	2,3,4,5,6,7,8,11,12,13,14,15,16,17
8	16	2,3,4,5,6,7,8,9,11,12,13,14,15,16,17,18
9	18	1,2,3,4,5,6,7,8,9,10,11,12,13,14,15,16,17,18

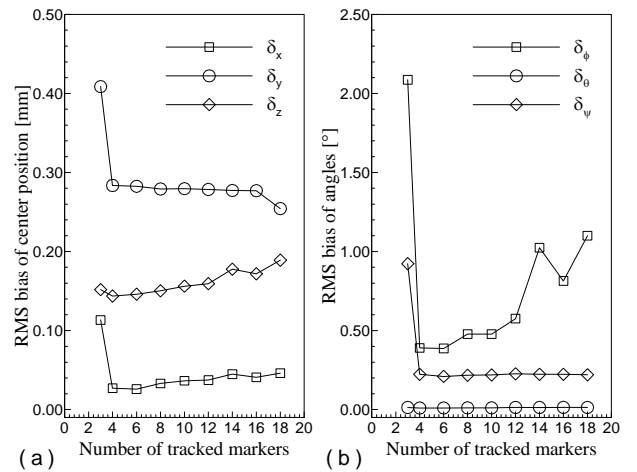


Figure 8. Influences of tracked marker number on RMS tracking biases: (a) model center coordinates, (b) angles of the tested model

When surface markers #3, #5, #8 and #14 are selected, the results of the 4-point tracking are given in Fig. 6a and 6b for model center coordinates (x_c, y_c, z_c) and angles (ϕ, θ, ψ) , respectively. The biases of the tracked motion variables from the given motion variables are shown in Fig. 7, i.e. $\sigma_x, \sigma_y, \sigma_z, \sigma_\phi, \sigma_\theta, \sigma_\psi$. The simulation results show that biases for determining the model center coordinates are smaller than 0.5 mm, and the biases for determining the pitch and yaw angles are smaller than 0.5° . The roll angle bias is much larger in the first and last quarter than in middle half of the tracking period because surface marker image #5 or #14 lost its contrast at the side of the model surface. In order to investigate the influence of the tracked surface marker number on the model motion tracking biases, nine groups of markers are selected and listed in Table I according to numbers defined in Fig. 5. The root-mean-square (RMS) values of tracking biases as shown in Fig. 7 are determined for tracking of each marker group, and the results are given in Fig. 8, i.e. $\delta_x, \delta_y, \delta_z, \delta_\phi, \delta_\theta, \delta_\psi$. Fig. 8 shows the influences of the number of tracked surface markers on the RMS bias errors of the motion tracking. It is shown that a minimum of three surface markers can be used to track the motion of the aerodynamic model but with obviously higher bias errors than those of more surface markers. When more than three tracking markers are used, the RMS biases for determining the model center coordinates are greatly reduced, i.e. <0.3 mm. The bias of the pitch and yaw angle are also very small when using at least 4 tracking markers. The RMS roll angle bias is as small as around 0.5° for tracking marker number 4~12, but it increase to about 1° for tracking markers of more than 12 because the uncertainty in markers #1, #2, #9, #10, #11 and #18 accumulate. The reason of an obviously higher roll angle bias level than the pitch and yaw angle bias level might be that the observed dimension in the radius direction is much smaller than that in the model axis direction.

IV. SUMMARY AND CONCLUSIONS

The presented stereo high-speed imaging system and the image processing and data reduction algorithms make it possible to investigate 3D motion of an aerodynamic model in a wind tunnel including variables of model center coordinates, roll angle, pitch angle, and yaw angle. A two-camera stereo imaging configuration is suggested to achieve high spatial and temporal resolution of the measurement. When properly distributed, a minimum of three surface markers can be used to track the motion of an aerodynamic model in wind tunnel tests; whereas four or more tracking markers enables a much higher accuracy. Too many markers may result in large tracking biases because uncertainty in the tracking markers may accumulate.

REFERENCES

- [1] V. Tiwari, M.A. Sutton, and S.R. McNeill, "Assessment of high speed imaging system for 2D and 3D deformation measurements: methodology development and validation," *Experimental Mechanics*, vol. 47, 2007, pp.561-579
- [2] L. Gui, T. Fink, Z. Cao, D. Sun, J.M. Seiner, and D.A. Streett, "Fire ant alate wingmotion data and numerical reconstruction," *Journal of Insect Science*, vol. 10, no. 19, 2010, available online: insectscience.org/10.19
- [3] K.Y. Cheung, and Y. Zhang, "Stereo imaging and analysis of combustion process in a gas turbine combustor," *Measurement Science and Technology*, vol. 17, 2006, pp. 3221-3228
- [4] T.T. Lu, and T.H. Chao, "A high-resolution and high-speed 3D imaging system and its application on ATR," *Proc. SPIE 6245, SPIE Symposium on Defense and Security, Optical Pattern Recognition XVII*, 2006
- [5] S. Sudo, K. Tsuyuki, and K. Kanno, "Wing characteristics and flapping behavior of flying Insects," *Experimental Mechanics*, Vol. 45, 2005, pp. 550-555
- [6] L. Ristroph, G.J. Berman, A.J. Bergou, Z.J. Wang, and I. Cohen, "Automated hull reconstruction motion tracking (HRMT) applied to sideways maneuvers of free-flying insects," *Journal of Experimental Biology*, vol. 212, 2009, pp. 1324-1335
- [7] A. K. Prasad, "Stereo particle image velocimetry," *Experiments in Fluids*, vol. 29, 2000, pp. 103-116
- [8] L. Gui, and J.M. Seiner, "An image tracking algorithm for time-resolved measurement of mini- and micro-scale motion of complex object," *Algorithms*, vol. 2, no. 1, 2009, pp.553-549
- [9] L. Gui, and J.M. Seiner, "Application of an image tracking algorithm in fire ant motion experiment," *Algorithms*, vol. 2, no. 2, 2009, pp.735-749